IEEE Access
Multidisciplinary | Rapid Review | Open Access Journal

Received October 23, 2019, accepted November 14, 2019, date of publication November 19, 2019,
date of current version December 2, 2019.

Digital Object Identifier 10.1109/ACCESS.2019.2954110

Initialized Model Reference Adaptive Control for Lower Limb Exoskeleton

MOHAMMAD SOLEIMANI AMIRI[1], RIZAUDDIN RAMLI[1], AND MOHD FAISAL IBRAHIM[2]
[1]Centre for Materials Engineering and Smart Manufacturing, Faculty of Engineering and Built Environment, Universiti Kebangsaan Malaysia, Bangi 43600, Malaysia
[2]Center for Integrated Systems Engineering and Advanced Technologies, Faculty of Engineering and Built Environment, Universiti Kebangsaan Malaysia, Bangi 43600, Malaysia

Corresponding author: Rizauddin Ramli (rizauddin@ukm.edu.my)

This work was supported in part by the Universiti Kebangsaan Malaysia (UKM) and in part by the Ministry of Education Malaysia under Research Grant FRGS/1/2017/TK03/UKM/02/4.

ABSTRACT In this paper, a Proportional-Integral-Derivative (PID) controller tuning scheme by Initialized Model Reference Adaptive Control (IMRAC) for a Lower Limb Exoskeleton (LLE) is presented. Mathematical expression of the LLE structure is determined using Lagrangian and Kirchoff's equations. The transfer function of the structure based on the physical features of the links, and actuators is established under Range of Motion (RoM) condition. The PID controller of the LLE is tuned in a closed-loop control system using Ziegler-Nichols (Z-N) for initializing parameters of IMRAC. Adjustment mechanism is a gradient based method for real-time adaptation of tuned PID controller. A Lyapunov function has been applied to confirm the stability of IMRAC. The proposed IMRAC shows faster convergence in comparison with conventional non-initialized model reference adaptive control. It can be ascertained the proposed tuning scheme is applicable for real-time tuning of PID controller of LLE.

INDEX TERMS Proportional-integral-derivative controller, lower limb exoskeleton, Lyapunov method, model reference adaptive control.

I. INTRODUCTION

In recent years, the demands for exoskeleton as a rehabilitation device have been increased, because of the growing population of elderly people and brain injuries such as stroke and Spinal Cord Injury (SCI) [1]–[3]. Therefore, development of the exoskeleton has been focused in assisting patients who lost their muscle stamina to recover their mobility function [4]–[6]. Lower Limb Exoskeleton (LLE) is a type of rehabilitation wearable robots, which is worn in parallel with patients' lower limb. The main application of LLE is to help physiotherapist for gait training [7]–[9]. Thus, designing a robust controller that can work under different conditions is essential for optimizing the LLE performance.

In this paper, Proportional-Integral-Derivative (PID) is developed as a controller in an adaptive control system. Combination of adaptive control and PID is used in several works [10], [11]. Aboud et al. [12] proposed multiple model adaptive control schemes, in which PID controller is selected as the controller for a mechatronic suspension system. Han et al. [13] developed a model-free based adaptive consists of intelligent Proportional-Integral (PI) controller, time-delay estimation, and adaptive sliding mode compensator for a 12 DoF LLE. Their control strategy in a simulated model was verified, and the stability was validated via Lyapunov theory. Wang et al. [14] combined fuzzy self-adaptive and variable-speed integral PID and presented fuzzy adaptive PID hybrid control strategy for a Multi-rotor Unmanned Aerial Vehicle (MUAV).

Many researches have been carried out to design an adaptive control system for LLE to withstand the external disturbance and noises. For instance, Zhang et. al. [15] employed a Neural Network (NN) and time-delay estimation to accomplish tracking trajectory for 10 Degree of Freedom (DoF) virtual prototype LLE. Its stability and effectiveness were compared with the results of the Proportional-Derivative (PD) controller. Zhu et al. [16] established a radial basis function of NN for controlling lower extremity exoskeleton by improving tracking performance and reducing interaction force between human and robot. They developed a robust non-linear integral sliding mode controller to improve the performance of their robot against uncertainties.

The associate editor coordinating the review of this manuscript and approving it for publication was Zheng H. Zhu.

Hou et al. [17] presented approach of Model-Free Adaptive Control (MFAC) and compared their results with data-driven PID control method for some simulation case studies, and they proved the effectiveness of MFAC by numerical analysis. Al-Mahbashi et al. [18] applied Lyapunov theory, and an adaptive control scheme to achieve hybrid function projective for synchronizing behavior between chaotic and hyperchaotic systems. Gains of Adaptive control are designed based on adaptive update law. The effectiveness of their proposed model is demonstrated by numerical example. Roman et al. [19] compared three data-driven techniques such as data-driven MFAC, Model-Free Control (MFC) and Virtual Reference Feedback Tuning (VRFT) to control representative non-linear Multi-Input-Multi-Output (MIMO) system. Wang et al. [20] proposed combination of adaptive NN control scheme and Nonlinear Model Predictive Control (NMPC) for a nonlinear system of multirate networked industrial process. They confirmed the effectiveness of their proposed control system in the simulation of continuous stirred tank reactor.

Several robust control systems for the LLE have been developed to handle the external disturbances and uncertainties [21]–[23]. For instance, He et al. [24] applied an adaptive neural network to estimate the unknown model of a two DoF rehabilitation robot by reducing the tracking error and effective interactions between human and robot. Wu et al. [25] presented an adaptive control scheme for a three DoF lower limb rehabilitation robot (LLRR) for adapting robot's uncertainties and overcome patients' disturbance. Their validation in simulation and experiments shows the effectiveness of the scheme in trajectory tracking problems. Ou et al. [26] developed Lyapunov-based adaptive fuzzy control to enable a human shank to track any continuous desired trajectory. Asl et al. [27] used an adaptive feed-forward NN, which works with position data of links in complying with the unknown non-linear dynamic of two DoF LLE. They validated their control system in simulation and experiment with satisfactory performance.

The main contribution of this paper is a new design of an adaptive control which tuned PID controller in real-time. The proposed tuning scheme can be used for a rehabilitation LLE. In addition, the novelty of this paper is to initialize an adaptive controller to reduce the trajectory error and to provide pre-computation before the prototype based on the mathematical model.

The control approach of this paper is Initialized Model Reference Adaptive Controller (IMRAC) which adopts PID controller, and a gradient based method known as MIT-rule for adjustment mechanism. A model reference transfer function of the plant was determined using Lagrangian and Kirchoff's equations. The gains of PID controller are tuned in closed-loop system using Ziegler-Nichols(Z-N). Tuned PID controller is used for initializing adjustment mechanism that is a gradient based method called MIT-rule. In addition, Lyapunov function is utilized to validate the stability of the control system. The proposed tuning scheme is tested on a 4 DoF LLE and compared with conventional non-initialized model reference adaptive controller.

II. DYNAMIC MODEL

Several methods such as Newton-Euler, Lagrangian, and inverse pendulum have been used to determine the dynamic equation of the multi-rigid-body robot [25], [28]. Among these methods, Lagrangian which is based on the analysis of energy of the model is widely used to determine the dynamic equation of the LLE. Figure 1 illustrates the simplified free body diagram in the sagittal plane. The LLE consists of two DoF in each leg [29].

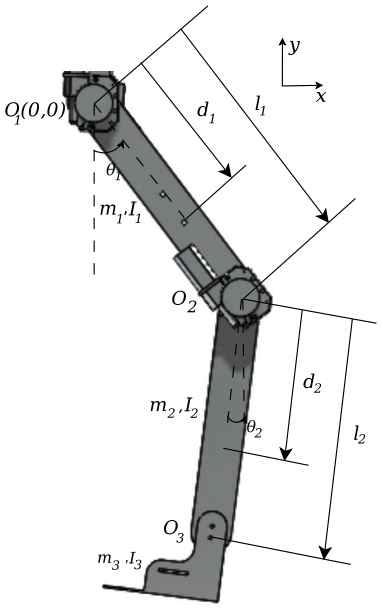

FIGURE 1. Free body diagram of two-DoF LLE leg.

The Lagrangian equation is given by,

$$La = E_k - E_p \tag{1}$$

$$T_{li} = \frac{d}{dt}\left(\frac{\partial La}{\partial \dot{\theta}_i}\right) - \left(\frac{\partial La}{\partial \theta_i}\right) \tag{2}$$

where, La is the Lagrangian function. T_{li} is the torque of femur and tibia, respectively. θ_i and $\dot{\theta}_i$, where $i = 1, 2$, are the trajectory angle and angular velocity. E_k and E_p are the total kinematic and potential energy respectively. In [25] the equations of E_p and E_k are determined as,

$$E_p = \sum_{i=1}^{2} m_i g y_i \tag{3}$$

$$E_k = \sum_{i=1}^{2} [\frac{1}{2} m_i (\dot{x}_i^2 + \dot{y}_i^2) + \frac{1}{2} I_i \dot{\theta}_i^2] \tag{4}$$

where, m_i is the mass of each link. I_i is the inertia; g is the gravity acceleration. In figure 1 O_1 is the coordinate origin. (x, y) is position of the Center of Gravity (CoG) which is

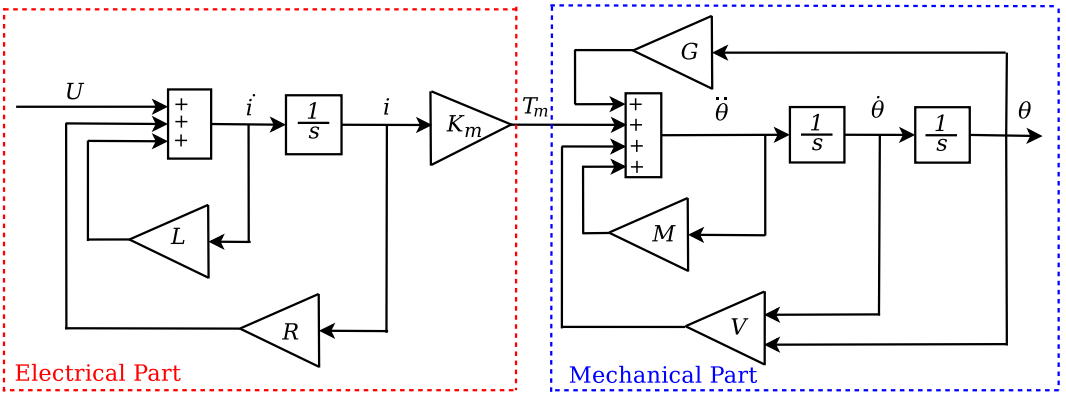

FIGURE 2. Block diagram of electrical and mechanical part of the LLE model.

derived by geometric relation, represented as,

$$x = \sum_{j=1}^{i-1} l_j sin(\theta_j) + d_i sin(\theta_i) \tag{5}$$

$$y = \sum_{j=1}^{i-1} l_j cos(\theta_j) + d_i cos(\theta_i) \tag{6}$$

where, l is the length of the links; d_i is the length from joint origin to the CoG. The state space dynamic equation of the links is given by,

$$T_l = M(\theta)\ddot{\theta} + V(\theta, \dot{\theta}) + G(\theta) \tag{7}$$

where, T_l is a 2×1 vector of the input torque toward the link; $\ddot{\theta}$ is the 2×1 angular acceleration vector; $M(\theta)$ is the 2×2 mass matrix; $V(\theta, \dot{\theta})$ is a 2×1 centrifugal and Coriolis vector; and $G(\theta)$ is a 2×1 gravity vector.

III. MOTOR MODEL

Direct Current (DC) motor is used as an actuator in the LLE which provides the required torque for joints to rotate [30], [31]. The DC motor includes electrical and mechanical parts that are rotary shaft, and armature [32].The electrical part is determined by Kirchhoff's voltage law given as follows,

$$U = L(\frac{di}{dt}) + Ri \tag{8}$$

where, L is the electric inductance; R and i are the resistance and the current of the DC motor; U is the input voltage. The torque as output of DC motor that rotates the mechanical part is proportioned to the current as follows,

$$T_m = K_m i \tag{9}$$

where, K_m and T_m are torque sensitivity and torque of DC motor, respectively. Dynamic equation of the shaft is expressed as follows,

$$T_{sh} = J\ddot{\theta} + B\dot{\theta} \tag{10}$$

where, J is the inertia of the shaft and B represents the friction of the DC motor. The mechanical part of the LLE is the rotary shaft of the DC motor which is connected to the link of the LLE. The output torque of DC motor, applied to the shaft and link is written as follows,

$$T_m = T_l + T_{sh} \tag{11}$$

Therefore, M, V, and G of equation 7 for the torque applied to the shaft and joints are expressed as follows,

$$M(\theta) = \begin{bmatrix} I_1 + m_2 l_1^2 + m_1 d_1^2 + J & m_2 l_1 d_2 cos(\theta_2 - \theta_1) \\ m_2 l_1 d_2 cos(\theta_2 - \theta_1) & I_2 + m_2 d_2^2 + J \end{bmatrix} \tag{12}$$

$$V(\theta, \dot{\theta}) = \begin{bmatrix} m_2 l_1 d_2 \dot{\theta}_2^2 sin(\theta_2 - \theta_1) + B\dot{\theta}_1 \\ m_2 l_1 d_2 \dot{\theta}_1 \dot{\theta}_2 sin(\theta_2 - \theta_1) + B\dot{\theta}_2 \end{bmatrix} \tag{13}$$

$$G(\theta) = \begin{bmatrix} m_1 g d_1 sin(\theta_1) + m_2 g l_1 sin(\theta_1) \\ m_2 g d_2 sin(\theta_2) \end{bmatrix} \tag{14}$$

Figure 2 represents the block diagram of electrical and mechanical parts of the LLE.

Transfer function of hip under Range of Motion (RoM) condition, in which while one joint is moving, the other joint is fixed [25], [33], is shown as follows.

$$G_1(s) = \frac{\theta_1(s)}{U_1(s)} = \frac{b}{a_{11}s^3 + a_{12}s^2 + a_{13}s + a_{14}} \tag{15}$$

where,

$$b = K_m \tag{16}$$

$$a_{11} = Ll_1^2 m_2 + Ld_1^2 m_1 + LJ + LI_1 \tag{17}$$

$$a_{12} = Rl_1^2 m_2 + Rd_1^2 m_1 + RJ + RI_1 + LB \tag{18}$$

$$a_{13} = l_1 Lgm_2 + Ld_1 gm_1 + RB \tag{19}$$

$$a_{14} = Rl_1 gm_2 + Rd_1 gm_1 \tag{20}$$

Similarly, transfer function of the knee in RoM condition is given as follows,

$$G_2(s) = \frac{\theta_2(s)}{U_2(s)} = \frac{b}{a_{21}s^3 + a_{22}s^2 + a_{23}s + a_{24}} \tag{21}$$

where,

$$a_{21} = Ld_2^2 m_2 + LJ + LI_2 \tag{22}$$

$$a_{22} = Rd_2^2 m_2 + RJ + RI_2 + LB \tag{23}$$

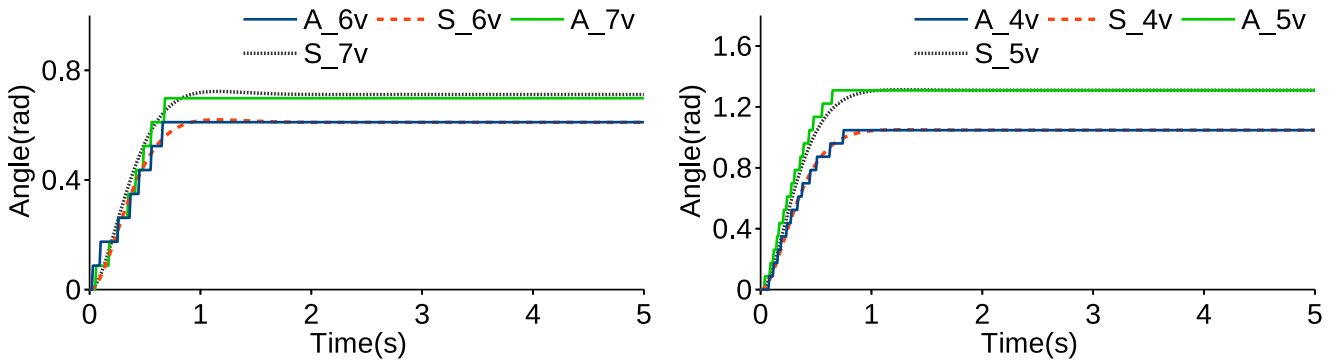

(a) hip (b) knee

FIGURE 3. Validation of transfer function.

TABLE 1. Transfer functions under RoM condition.

Component	transfer function
hip	$G_1(s) = \frac{52.1017}{0.001s^3+0.4396s^2+3.1604s+8.9409}$
knee	$G_2(s) = \frac{52.1017}{0.001s^3+0.1321s^2+1.1838s+3.4727}$

$$a_{23} = Ld_2d_2gm_2 + RB \tag{24}$$

$$a_{24} = Rd_2gm_2 \tag{25}$$

Parameters of the transfer functions of hip and knee are positive and constant values. These parameters are identified using parameter estimation TOOLBOX of MATLAB that set values for the parameters optimally, until the error between the experimentally measured and calculated trajectory converge to almost zero. Table 1 exhibits the transfer function of hip, and knee under RoM condition.

Figures 3a and 3b compare the output of the transfer function in an open-loop and actual trajectory that is measured using an encoder. For transfer function and actual the input is voltage, and the output is the angular trajectory of the joint. The output of transfer function is shown by "$S-$" and actual one is expressed by "$A-$". For both hip and knee, the simulated graphs follow the actual one that represents the validation of transfer functions of hip and knee.

IV. DESIGN OF IMRAC

A. PID CONTROLLER

PID controller is one of the most popular controllers in industry because of its ease of implementation in a control system [34]–[36]. This controller consists of three parameters, which are proportional, integral, and derivative terms, denoted by K_p, K_i, and K_d, respectively. Figure 4 illustrates the block diagram of PID controller.

Laplace transfer function of PID controller is given as follows,

$$C(s) = \frac{U}{e} = K_p + \frac{1}{s}K_i + K_d s \tag{26}$$

$$C(s) = \frac{K_p s + K_i + K_d s^2}{s} \tag{27}$$

Figure 5 illustrates the closed-loop control system.

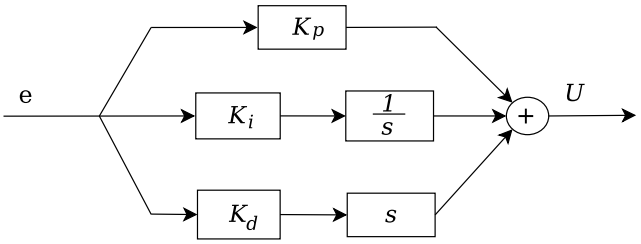

FIGURE 4. Block diagram of PID controller.

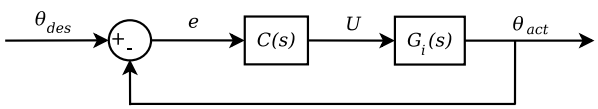

FIGURE 5. closed-loop control system.

θ_{des} and θ_{act} are desired and actual trajectory. In addition, e represents the error of the control system, which is the difference of the actual and desired trajectory.

$$e = \theta_{des} - \theta_{act} \tag{28}$$

Transfer function of closed-loop control system as the following equation.

$$\frac{\theta_{act}}{\theta_{des}} = \frac{G_i C(s)}{1 + G_i C(s)} \tag{29}$$

$G_i(s)$ is transfer function of hip and knee, while $i = 1$ and $i = 2$ respectively.

The PID parameters are tuned by Z-N method, which is the classical observation technique of tuning. The pseudo code of the Z-N is explained in Algorithm 1.

In the Algorithm 1, K_u is the K_p, while the K_i and K_d are zero. K_u is initialized from zero and increased by K_s as step value in each iteration until a stable oscillation is obtained. The final value of K_u is ultimate gain distinguished by K_{cr} and T_u is measured as the ultimate oscillation period. The parameters of PID controller are expressed as follows,

$$K_p = 0.6 \times K_{cr} \tag{30}$$

$$K_i = \frac{1.2 \times K_{cr}}{T_u} \tag{31}$$

Algorithm 1 Algorithm of Z-N

start
set $K_i = 0$;
set $K_d = 0$;
set $K_p = K_u$;
initialize K_u;
set step value for as K_s
while observe stable oscillation **do**;
    set value for K_u;
    $K_u = K_u + K_s$;
end while
set $K_u = K_{cr}$;
calculate oscillation period as T_u;
calculate K_p, K_i, and K_d
end

TABLE 2. Parameters of the PID controller.

	K_p	K_i	K_d
hip	5.2522	9.9557	0.3898
knee	2.1933	3.9952	0.1823

$$K_d = \frac{3 \times K_{cr} \times T_u}{40} \tag{32}$$

Table 2 illustrates the gains of the PID for each joint.

The proportional, integral, and derivative gains for hip are 5.25224, 9.9557, and 0.3898, respectively. Similarly, these values for knee are 2.1933, 3.9952, and 0.1823.

Figure 6 shows the trajectory angle of the hip and knee joint in a closed-loop controller system. Performance of the PID controller tuned by Z-N is verified in the closed-loop control system.

B. ADAPTATION LAW

In this paper, IMRAC approach is used for designing an adaptive control. IMRAC consists of a plant, an adjustment mechanism that set controller parameters in real-time, a model reference that provides ideal behavior of the control system [37], [38]. The initial values of PID controller are set from the closed-loop control system. Figure 7 shows block diagram of adaptive control.

θ_m and $\acute{e}$ represent the trajectory of model reference and tracking error, which is the difference between θ_m and the actual trajectory.

$$\acute{e} = \theta_{act} - \theta_m \tag{33}$$

Model reference is estimated in such a way that produces the ideal trajectory of the joints and is in the same order with the closed-loop transfer function.

$$G_m(s) = \frac{s^2 + b_{m_1}s + b_{m_2}}{s^4 + a_{m_1}s^3 + a_{m_2}s^2 + a_{m_3}s + a_{m_4}} \tag{34}$$

C. ADJUSTMENT MECHANISM

Parameters of the tuned PID controller are adapted by an adjustment mechanism to minimize tracking error. MIT-rule

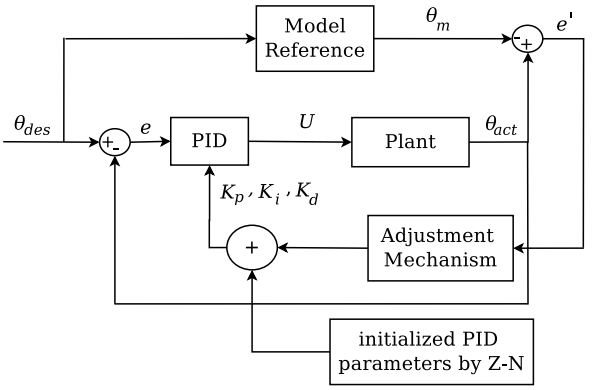

FIGURE 7. Configuration of IMRAC.

is an efficient method based on gradient approach to minimize the tracking error [39], [40]. The cost function is given as follows,

$$J(K_j) = \frac{\acute{e}^2}{2} \quad j = p, i, d \tag{35}$$

K_j is parameters of PID controller, which should be adjusted to minimize the cost function. Therefore, the change of the K_j in negative direction of the gradient of $J(K_j)$,

$$\frac{dK_j}{dt} = -\gamma \frac{\partial J}{\partial K_j} \tag{36}$$

$$\frac{dK_j}{dt} = -\gamma_j e' \frac{\partial e'}{\partial K_j} = -\gamma_i e' \frac{\partial \theta_{act}}{\partial K_j} \tag{37}$$

where, $\frac{\partial e'}{\partial K_j}$ is sensitivity derivatives of tracking error; γ represents speed of adaption. From equation 29, θ_{act} is given as follows,

$$\theta_{act} = \frac{G_i C(s)}{1 + G_i C(s)} \theta_{des} \tag{38}$$

The symbolic transfer function of G_i can be expressed as follows,

$$G_i = \frac{b}{s^3 + a_1 s^2 + a_2 s + a_3} \tag{39}$$

By substituting equations 27 and 39 in equation 38, θ_{act} is written as follows,

$$\theta_{act} = \frac{b(K_d s^2 + K_p s + K_i)}{s^4 + a_1 s^3 + (a_2 + bK_d)s^2 + (a_3 + bK_p)s + bK_i} \theta_{des} \tag{40}$$

Consequently, by assuming,

$$a_{m1} = a_1 \quad a_{m2} = a_2 + bK_d \quad a_{m3} = a_3 + bK_p \tag{41}$$

$$a_{m4} = bK_p s + bK_i \tag{42}$$

the partial of θ_{act} over K_j while $j = p, i, d$ is given as follows,

$$\frac{\partial \theta_{act}}{\partial K_p} = \frac{bes}{s^4 + a_{m_1}s^3 + a_{m_2}s^2 + a_{m_3}s + a_{m_4}} \tag{43}$$

$$\frac{\partial \theta_{act}}{\partial K_i} = \frac{be}{s^4 + a_{m_1}s^3 + a_{m_2}s^2 + a_{m_3}s + a_{m_4}} \tag{44}$$

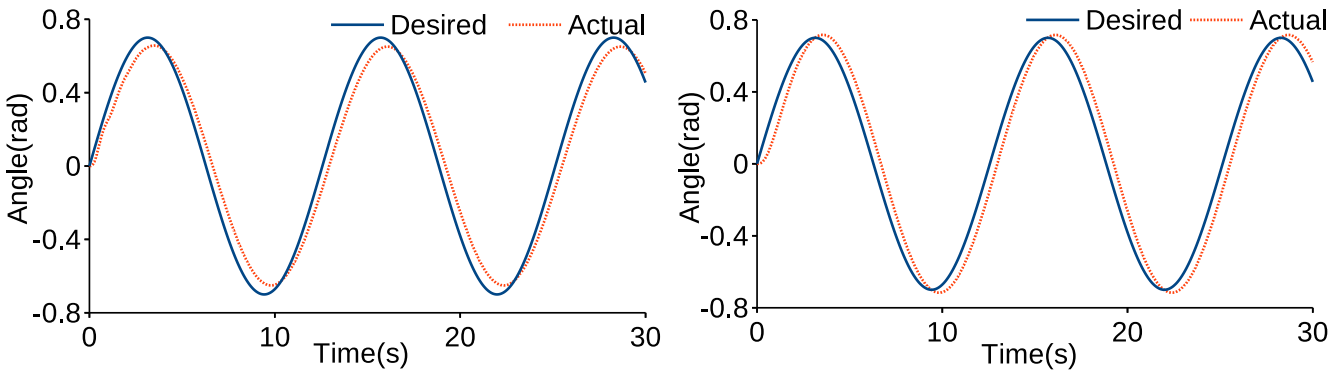

(a) hip (b) knee

FIGURE 6. Validation of PID controller.

$$\frac{\partial \theta_{act}}{\partial K_d} = \frac{bes^2}{s^4 + a_{m_1}s^3 + a_{m_2}s^2 + a_{m_3}s + a_{m_4}} \tag{45}$$

By substitution of equations 43,44, and 45 in equation 37 and its integral in Laplace, the parameters of PID controller are determined as follows,

$$K_P = -\gamma_p e' \frac{bes}{s^4 + a_{m_1}s^3 + a_{m_2}s^2 + a_{m_3}s + a_{m_4}} + c_p \tag{46}$$

$$K_i = -\gamma_i e' \frac{be}{s^4 + a_{m_1}s^3 + a_{m_2}s^2 + a_{m_3}s + a_{m_4}} + c_i \tag{47}$$

$$K_d = -\gamma_d e' \frac{bes^2}{s^4 + a_{m_1}s^3 + a_{m_2}s^2 + a_{m_3}s + a_{m_4}} + c_d \tag{48}$$

where, c_p, c_i, and c_d represent the initial values of the PID parameters that are selected from the tuned PID controller using Z-N. By selecting the initial value the error and the computational time will be reduced.

V. LYAPUNOV STABILITY

In this study, Lyapunov function is utilized in validation the stability of the control system. Equation of plant which consists of the electrical and mechanical parts of the LLE is given as follows,

$$\dddot{y} + a_1\ddot{y} + a_2\dot{y} + a_3 y = bu \tag{49}$$

The state space variables are assumed as follows,

$$X_1 = y \tag{50}$$

$$X_2 = \dot{y} = \dot{X}_1 \tag{51}$$

$$X_3 = \ddot{y} = \dot{X}_2 \tag{52}$$

State space of equation 49 is given as,

$$\dot{X}_3 = \dddot{y} = -a_1X_3 - a_2X_2X_2 - a_3X_1 + bu \tag{53}$$

From equations 52 and 53, the control system is donated as,

$$\begin{bmatrix} \dot{X}_1 \\ \dot{X}_2 \\ \dot{X}_3 \end{bmatrix} = -\begin{bmatrix} 0 & 1 & 0 \\ 0 & 0 & 1 \\ a_1 & a_2 & a_3 \end{bmatrix} \begin{bmatrix} X_1 \\ X_2 \\ X_3 \end{bmatrix} + \begin{bmatrix} 0 \\ 0 \\ b \end{bmatrix} u \tag{54}$$

or

$$\dot{X} = -AX + Bu \tag{55}$$

$$y = \begin{bmatrix} 1 & 0 & 0 \end{bmatrix} \begin{bmatrix} X_1 \\ X_2 \\ X_3 \end{bmatrix} = CX \tag{56}$$

Similarly for reference model, the state space can be determined as follows

$$\dot{X_m} = -A_m X_m + B_m r \tag{57}$$

where, r represents the reference of the control system which is θ_{act}. The controller of the system is given as,

$$\frac{u}{e} = K_p + \frac{1}{s}K_i + K_d s \tag{58}$$

$$e = r - CX \tag{59}$$

$$u = \begin{bmatrix} 1 & \frac{1}{s} & s \end{bmatrix} \begin{bmatrix} k_p \\ \frac{k_i}{s} \\ k_d s \end{bmatrix} (r - CX) = OPr - OPCX \tag{60}$$

In this paper, the MIT-rule can be expressed from equations 46,47, and 48 as,

$$\dot{k_p} = -\gamma_p e' \frac{s(r - CX)}{r} \tag{61}$$

$$\dot{k_i} = -\gamma_i e' \frac{(r - CX)}{r} \tag{62}$$

$$\dot{k_d} = -\gamma_d e' \frac{s^2(r - CX)}{r} \tag{63}$$

where equations 61, 62, and 63 can be written as follows,

$$\begin{bmatrix} \dot{k_p} \\ \dot{k_i} \\ \dot{k_d} \end{bmatrix} = \begin{bmatrix} -\frac{\gamma_p s}{r} \\ -\frac{\gamma_i}{r} \\ -\frac{\gamma_d s^2}{r} \end{bmatrix} e'(r - CX) \tag{64}$$

By substitution of $\dot{P} = \begin{bmatrix} \dot{k_p} \\ \dot{k_i} \\ \dot{k_d} \end{bmatrix}$ and $\Gamma = \begin{bmatrix} -\frac{\gamma_p s}{r} \\ -\frac{\gamma_i}{r} \\ -\frac{\gamma_d s^2}{r} \end{bmatrix}$, the adjustment mechanism is expressed as follows,

$$\dot{P} \approx \Gamma e'(r - CX) \approx \Gamma e' r - \Gamma e' CX \tag{65}$$

Equation 60 is substituted in equation 55

$$\dot{X} = -AX + B(OPr - OPCX) = -(A + BOPC)X + BOPr \tag{66}$$

By comparing equations 66 and 57, the parameters of model reference can be estimated as follows,

$$A_m = A + BO\hat{P}C \tag{67}$$
$$B_m = BO\hat{P} \tag{68}$$

where $\hat{P}$ is an estimation of the controller parameters. The tracking error is given as,

$$e' = X - X_m \tag{69}$$

then,

$$\dot{e'} = \dot{X} - \dot{X_m} \tag{70}$$
$$\dot{e'} = -(A + BOPC)X + BOPr + A_m X_m - B_m r \tag{71}$$

X_m can be substituted by $X - e'$. Furthermore, by substitution equation 68 in the equation 71, $\dot{e'}$ can be written as,

$$\dot{e'} = -(A + BOPC)X + BOPr + (A + BO\hat{P}c)(X - e') - BO\hat{P}r \tag{72}$$
$$\dot{e'} = (-A - BOPC + A + BO\hat{P}C)X + (BOP - BO\hat{P})r - Ae' \tag{73}$$
$$\dot{e'} = -BO(P - \hat{P})CX + BO(P - \hat{P})r - Ae' \tag{74}$$

Assuming that $p - \hat{p}$ is θ, then equation 73 is given as,

$$\dot{e'} = -BO\theta CX + BO\theta r - Ae' \tag{75}$$

Therefor, the candidate Lyapunov equation is given as,

$$v = \frac{1}{2}(\dot{e'} + \frac{1}{\lambda}\theta^2) \tag{76}$$
$$\dot{v} = \dot{e'}e' + \frac{1}{\lambda}\dot{\theta}\theta \tag{77}$$

where, $\dot{\theta} = \dot{P}$. By substitution of equation 65 and 73 in the equation 77, derivative of the Lyapunov function can be expressed as,

$$\dot{v} = e'(-BO\theta CX + BO\theta r - Ae') + \frac{1}{\lambda}\theta(\Gamma e' r - \Gamma e' CX) \tag{78}$$

$$\dot{v} = (-BO\theta C - \acute{e}\frac{1}{\lambda}\theta\Gamma C)X + (BO\theta\acute{e} + \frac{1}{\lambda}\theta\Gamma\acute{e})r - A\acute{e}^2 \tag{79}$$

For $\lambda = -[BO]^{-1}\Gamma$,

$$\dot{v} = -A\acute{e}^2 \tag{80}$$

where, $[BO]$ and A, which are a 3×3 matrix should be a positive definite matrix. Because the derivative of Lyapunov function is negative, the system is stable [41].

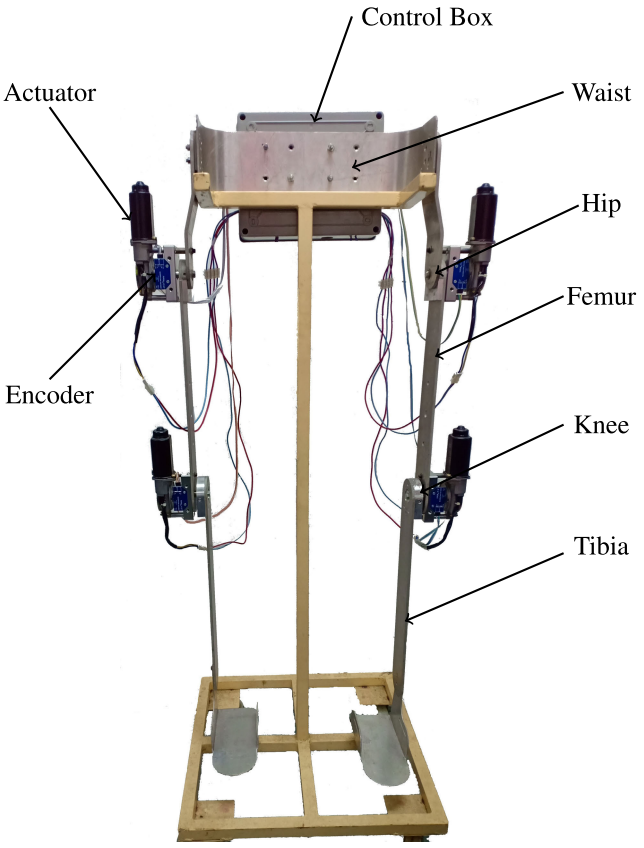

FIGURE 8. Components of LLE.

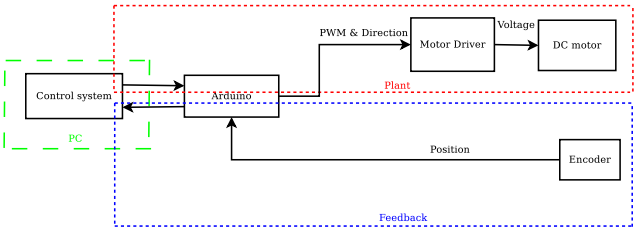

FIGURE 9. Hardware configuration.

VI. EXPERIMENT

The LLE consists of the control box, which is connected to the waist, and two legs, connected to the backpack frame. Each leg is composed of two links as femur and tibia. Femur is attached to the backpack frame by the hip joint which is a revolute joint. The same connection is assembled for tibia to the femur. The actuator of the LLE is brushed permanent magnet DC motor and gearbox. DC motor and a gearbox are connected in parallel with the links. The gearbox reduces the speed of the motor and increases the torque. Figure 8 illustrates components of the LLE.

Figure 9 shows hardware configuration, including micro-controller, encoder, and motor driver. A quadrature encoder is located at the output shaft of gearbox and position of the joint is sent to the control system as feedback. Arduino Mega 2560 microcontroller is employed to communicate with the

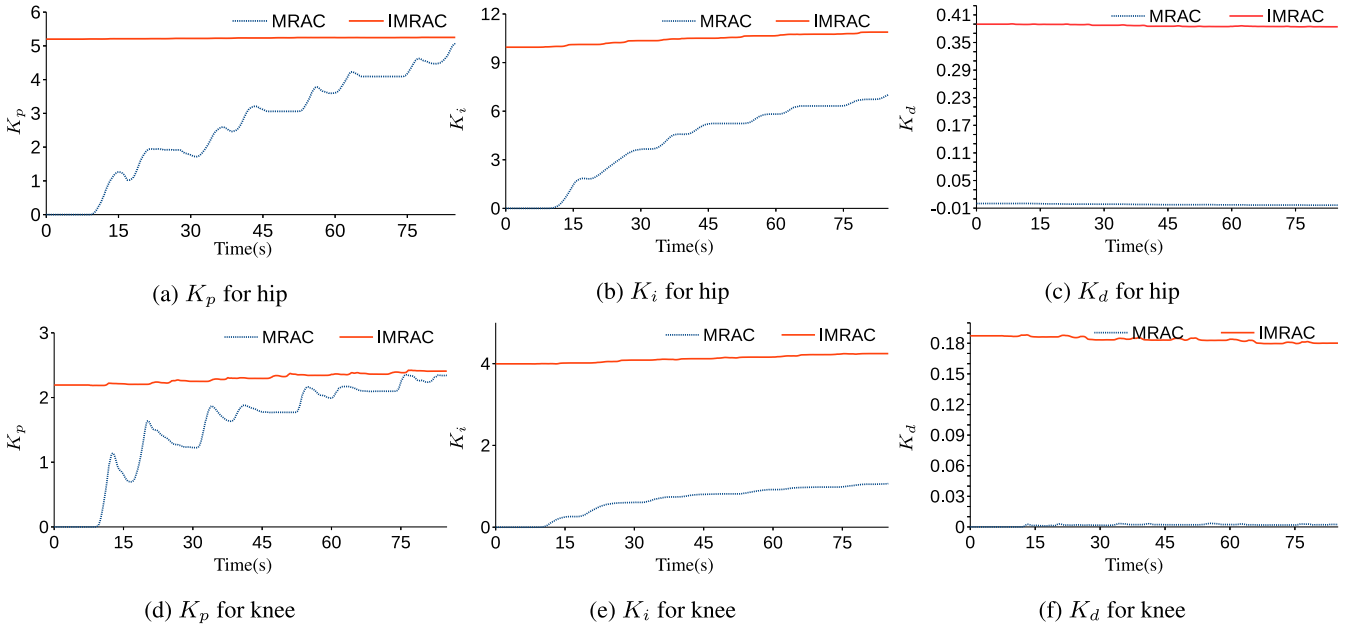

(a) K_p for hip (b) K_i for hip (c) K_d for hip

(d) K_p for knee (e) K_i for knee (f) K_d for knee

FIGURE 10. Parameters of PID controller.

hardwares and PC. A motor driver is utilized for each motor to control voltage and movement direction of the DC motors. The input of the control system toward Arduino is Pulse Width Modulation (PWM) which is bounded from 0 to 255. In addition, direction data are sent to Arduino, which is zero when the voltage to the plant is positive, and it is one when the voltage toward the plant is negative. Motor driver is utilized to convert direction and PWM data to clockwise and counterclockwise rotation by changing the positive and negative input voltage to DC motor, which can tolerate maximum 12V.

VII. RESULTS AND DISCUSSION

The performance of IMRAC is tested with the LLE and compared with conventional Model Reference Adaptive Control (MRAC). MATLAB-SIMULINK is employed for controlling and communication with the LLE. A periodic trajectory is defined as reference of the control system for each joint.

Figure 10 exhibits the changes of K_p, K_i, and K_d for both IMRAC and MRAC for hip and knee. The initial parameters for MRAC are set to zero and raised while, PID parameters for IMRAC are kept remained as a constant value without significant changes, because, they are initialized by Z-N shown in table 2 based on the mathematical model of the LLE expressed at the table 1. The initial values are used in adjustment mechanism of IMRAC, which are represented in equations 46, 47, 48.

Figures 11a and 11b show the comparison of tracking trajectories of the IMRAC and MRAC for hip and knee joint, respectively. The actual trajectory of the MIRAC response faster to the desired trajectory than MRAC because the adjustment mechanism is initialized. Although, it is not necessary for IMRAC to search PID parameters from zero, it can adapt PID parameters based on comparing the output of control system and reference model. In the figures 11c and 11d *E_MRAC* and *E_IMRAC* stand for angular trajectory error of hip and knee, respectively. *E_MRAC* starts from greater error that *E_IMRAC* and gradually decreases for both joints, while still stays greater than *E_MRAC* at the end of the time period, because initialization of IMRAC causes fast convergence.

TABLE 3. Error of trajectory for each joint.

Joint	MRAC			IMRAC		
	ME	AE	RMS	ME	AE	RMS
Hip	0.2	0.079	0.0929	0.0488	0.0079	0.0131
Knee	0.3450	0.0823	0.1074	0.1096	0.0199	0.0238

Figure 12 illustrates the voltage of each joint, which are periodic graphs. The voltages are the output signal of the controller to Arduino. For IMRAC, voltage is started sending to LLE from initial times, while for MRAC, it takes time that controller set parameters for PID and start sending voltage. In addition, voltage consumption of hip is greater than knee because the actuator of hip carries the weight of femur and tibia while the knee actuator only handles the weight of the tibia.

Table 3 exhibits numerical analysis of trajectory error of each joint in both IMRAC and MRAC. Maximum Error (*ME*) of hip and joint by MRAC shows higher values compared to IMRAC, which exhibits the efficiency of the proposed scheme. On the other hand, Average Error (*AE*) follows the same trend with *ME* and does not exceed 0.05. Similarly, for Root Mean Square (*RMS*) the values for IMRAC are far less than MRAC for each joint.

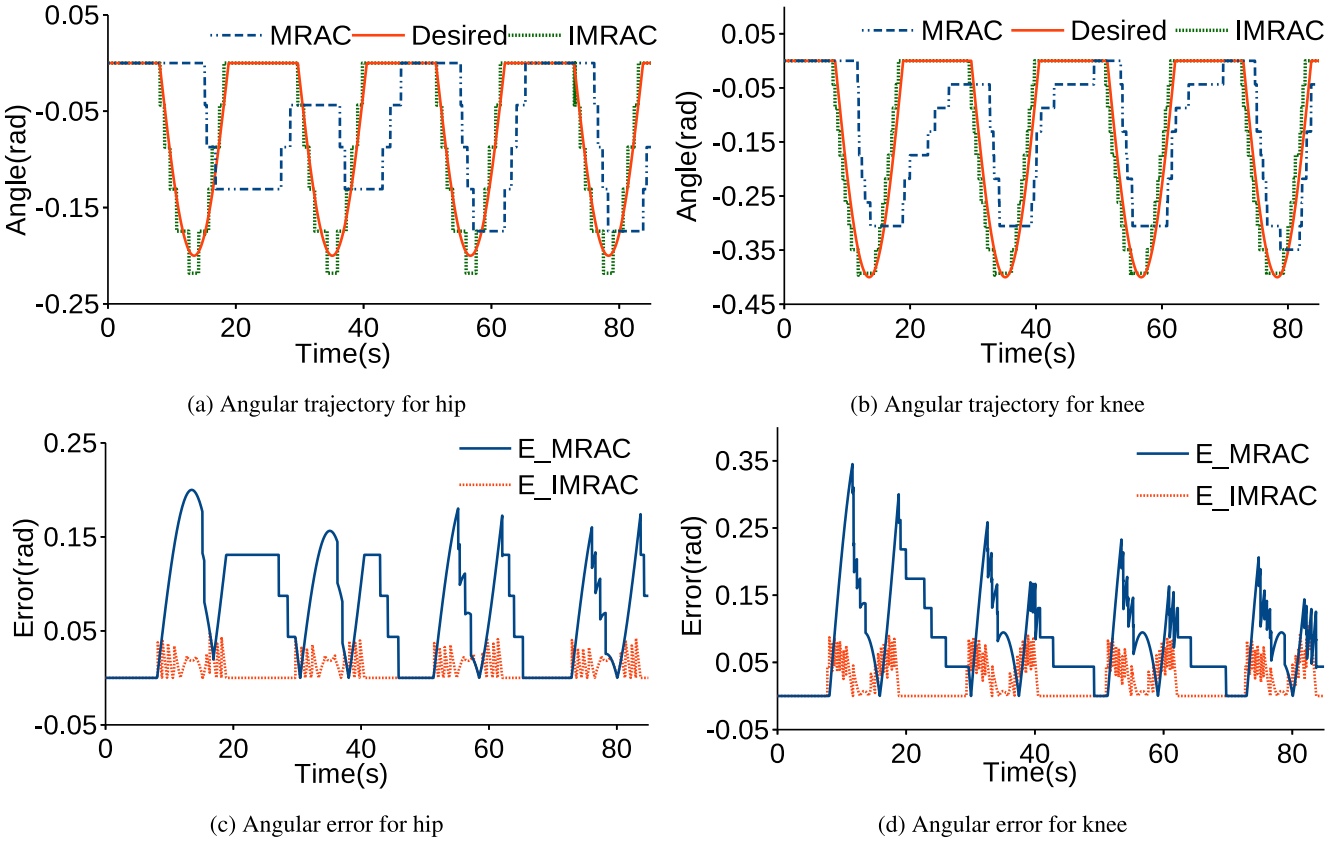

(a) Angular trajectory for hip

(b) Angular trajectory for knee

(c) Angular error for hip

(d) Angular error for knee

FIGURE 11. Angular trajectory and its error of each joint.

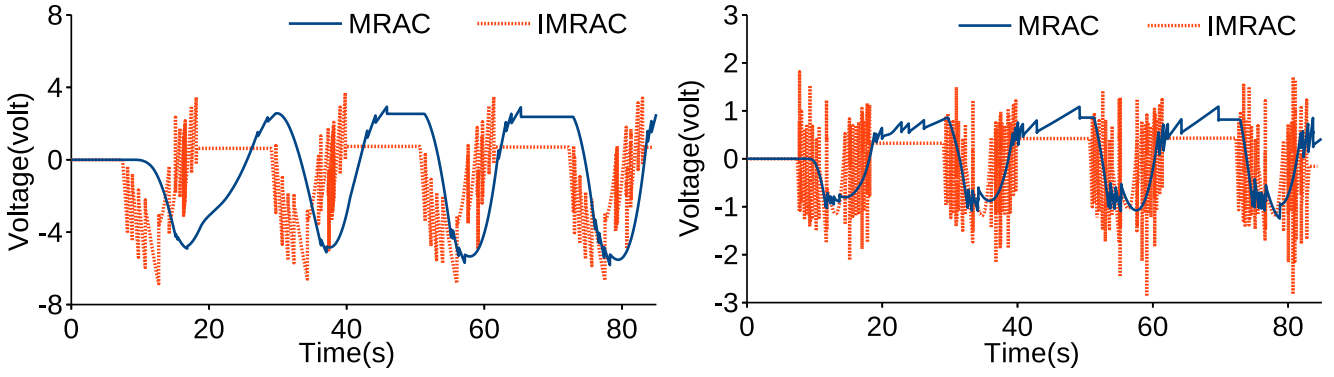

(a) hip

(b) knee

FIGURE 12. Actual voltage of each joint.

VIII. CONCLUSION

In this paper, IMRAC was used to control a LLE. PID was employed as controller and MIT-rule were used as an adjustment mechanism to adapt parameters of PID controller for a two DoF rehabilitation LLE. The dynamic equations of the LLE and DC motor as an actuator were determined by using Lagrangian and Kirchhoff's equations. Furthermore, transfer functions of the DC motor and the links of the LLE were determined based on the physical features of the LLE in the RoM condition. The transfer functions were developed in the closed-loop control system to tune PID controller using Z-N. The parameters of the tuned PID controller were implemented as initial values in the adjustment mechanism. The comparison between the results of the IMRAC and conventional MRAC, shows the IMRAC converged faster and consumed less computational time than MRAC.

The proposed control system can be used in LLE as a gait training robot for rehabilitation purpose. However, the control

system has not been validated in the LLE with adjustment links or different actuators. In addition, the LLE has not been tested in the environment with disturbances and different tasks of rehabilitation. Based on the limitations, the controller can be set to be more robust to the disturbances and the control system can be applied in different frames of the LLE under various conditions with other kinds of actuators.

REFERENCES

[1] A. J. Young and D. P. Ferris, "State of the art and future directions for lower limb robotic exoskeletons," *IEEE Trans. Neural Syst. Rehabil. Eng.*, vol. 25, no. 2, pp. 171–182, Feb. 2017.

[2] D. Ao, R. Song, and J. Gao, "Movement performance of human–robot cooperation control based on EMG-driven hill-type and proportional models for an ankle power-assist exoskeleton robot," *IEEE Trans. Neural Syst. Rehabil. Eng.*, vol. 25, no. 8, pp. 1125–1134, Aug. 2017.

[3] S. Wang, L. Wang, C. Meijneke, E. van Asseldonk, T. Hoellinger, G. Cheron, Y. Ivanenko, V. La Scaleia, F. Sylos-Labini, M. Molinari, F. Tamburella, I. Pisotta, F. Thorsteinsson, M. Ilzkovitz, J. Gancet, Y. Nevatia, R. Hauffe, F. Zanow, and H. van der Kooij, "Design and control of the MINDWALKER exoskeleton," *IEEE Trans. Neural Syst. Rehabil. Eng.*, vol. 23, no. 2, pp. 277–286, Mar. 2015.

[4] B. S. Rupal, S. Rafique, A. Singla, E. Singla, M. Isaksson, and G. S. Virk, "Lower-limb exoskeletons: Research trends and regulatory guidelines in medical and non-medical applications," *Int. J. Adv. Robotic Syst.*, vol. 14, no. 6, pp. 1–27, 2017.

[5] K. Kong and D. Jeon, "Design and control of an exoskeleton for the elderly and patients," *IEEE/ASME Trans. Mechatronics*, vol. 11, no. 4, pp. 428–432, Aug. 2006.

[6] M. Franz, L. Richner, M. Wirz, A. von Reumont, U. Bergner, T. Herzog, W. Popp, K. Bach, N. Weidner, and A. Curt, "Physical therapy is targeted and adjusted over time for the rehabilitation of locomotor function in acute spinal cord injury interventions in physical and sports therapy," *Spinal Cord*, vol. 56, no. 2, pp. 158–167, 2018.

[7] C.-H. Wu, H.-F. Mao, J.-S. Hu, T.-Y. Wang, Y.-J. Tsai, and W.-L. Hsu, "The effects of gait training using powered lower limb exoskeleton robot on individuals with complete spinal cord injury," *J. NeuroEng. Rehabil.*, vol. 15, no. 1, 2018, Art. no. 14.

[8] V. Bartenbach, M. Gort, and R. Riener, "Concept and design of a modular lower limb exoskeleton," in *Proc. 6th IEEE Int. Conf. Biomed. Robot. Biomechatronics (BioRob)*, Jun. 2016, pp. 649–654.

[9] N. Aliman, R. Ramli, and S. M. Haris, "Modeling and co-simulation of actuator control for lower limb exoskeleton," in *Proc. 3rd Int. Conf. Control Robot. Eng. (ICCRE)*, Apr. 2018, pp. 94–98.

[10] S. Zihao, W. Bin, and Z. Ting, "Trajectory tracking control of a spherical robot based on adaptive PID algorithm," in *Proc. Chin. Control Decis. Conf. (CCDC)*, Jun. 2019, pp. 5171–5175.

[11] X. Wu, J. Wu, and D. Li, "Designation and simulation of environment laboratory temperature control system based on adaptive fuzzy PID," in *Proc. IEEE 3rd Adv. Inf. Technol., Electron. Autom. Control Conf. (IAEAC)*, Oct. 2018, pp. 583–587.

[12] W. S. Aboud, S. M. Haris, and Y. Yaacob, "Weighted multiple model adaptive PID control for a mechatronic suspension system," *ICIC Exp. Lett.*, vol. 8, no. 8, pp. 2335–2341, 2014.

[13] S. Han, H. Wang, and Y. Tian, "Model-free based adaptive nonsingular fast terminal sliding mode control with time-delay estimation for a 12 DOF multi-functional lower limb exoskeleton," *Adv. Eng. Softw.*, vol. 119, pp. 38–47, May 2018.

[14] R. Wang and Z. Zhang, "Fuzzy adaptive PID hybrid control for airborne platform mounted on mUAV," in *Proc. IEEE Inf. Technol., Netw., Electron. Autom. Control Conf. (ITNEC)*, vol. 4, May 2016, pp. 737–741.

[15] X. Zhang, H. Wang, Y. Tian, L. Peyrodie, and X. Wang, "Model-free based neural network control with time-delay estimation for lower extremity exoskeleton," *Neurocomputing*, vol. 272, pp. 178–188, Jan. 2018.

[16] S. Zhu, X. Jin, B. Yao, Q. Chen, X. Pei, and Z. Pan, "Non-linear sliding mode control of the lower extremity exoskeleton based on human–robot cooperation," *Int. J. Adv. Robotic Syst.*, vol. 13, no. 5, pp. 1–10, 2016.

[17] Z. Hou and S. Xiong, "On model-free adaptive control and its stability analysis," *IEEE Trans. Autom. Control*, vol. 64, no. 11, pp. 4555–4569, Nov. 2019.

[18] G. Al-Mahbashi, M. S. Noorani, and S. A. Bakar, "Adaptive hybrid function projective synchronization in drive-response discrete networks with delay coupling," *AIP Conf. Proc.*, vol. 1830, no. 1, 2017, Art. no. 020013.

[19] R.-C. Roman, M.-B. Radac, and R.-E. Precup, "Multi-input–multi-output system experimental validation of model-free control and virtual reference feedback tuning techniques," *IET Control Theory Appl.*, vol. 10, no. 12, pp. 1395–1403, Aug. 2016.

[20] T. Wang, H. Gao, and J. Qiu, "A combined adaptive neural network and nonlinear model predictive control for multirate networked industrial process control," *IEEE Trans. Neural Netw. Learn. Syst.*, vol. 27, no. 2, pp. 416–425, Feb. 2016.

[21] C. Yang, G. Ganesh, S. Haddadin, S. Parusel, A. Albu-Schäffer, and E. Burdet, "Human-like adaptation of force and impedance in stable and unstable interactions," *IEEE Trans. Robot.*, vol. 27, no. 5, pp. 918–930, Oct. 2011.

[22] S. Elferik and I. H. Imran, "Control of nonholonomic mobile robot based on immersion and invariance adaptive control," in *Proc. IEEE 12th Int. Multi-Conf. Syst., Signals Devices (SSD)*, Mar. 2015, pp. 1–5.

[23] L. Gracia, J. E. Solanes, P. Muñoz-Benavent, A. Esparza, J. V. Miro, and J. Tornero, "Cooperative transport tasks with robots using adaptive non-conventional sliding mode control," *Control Eng. Pract.*, vol. 78, pp. 35–55, Sep. 2018.

[24] W. He, S. S. Ge, Y. Li, E. Chew, and Y. S. Ng, "Neural network control of a rehabilitation robot by state and output feedback," *J. Intell. Robot. Syst.*, vol. 80, no. 1, pp. 15–31, 2015.

[25] J. Wu, J. Gao, R. Song, R. Li, Y. Li, and L. Jiang, "The design and control of a 3DOF lower limb rehabilitation robot," *Mechatronics*, vol. 33, pp. 13–22, Feb. 2016.

[26] Y. Ou, Z. Li, G. Li, and C.-Y. Su, "Adaptive fuzzy tracking control of a human lower limb with an exoskeleton," in *Proc. IEEE Int. Conf. Robot. Biomimetics (ROBIO)*, Dec. 2012, pp. 1937–1942.

[27] H. J. Asl, T. Narikiyo, and M. Kawanishi, "Neural network-based bounded control of robotic exoskeletons without velocity measurements," *Control Eng. Pract.*, vol. 80, pp. 94–104, Nov. 2018.

[28] T. H. Baluch, A. Masood, J. Iqbal, U. Izhar, and U. S. Khan, "Kinematic and dynamic analysis of a lower limb exoskeleton (Version 9496)," 2012, doi: 10.5281/zenodo.1072880.

[29] M. S. Amiri, R. Ramli, and M. F. Ibrahim, "Hybrid design of PID controller for four DoF lower limb exoskeleton," *Appl. Math. Model.*, vol. 72, pp. 17–27, Aug. 2019.

[30] Munadi, M. A. Akbar, T. Naniwa, and Y. Taniai, "Model reference adaptive control for DC motor based on Simulink," in *Proc. 6th Int. Annu. Eng. Seminar (InAES)*, Aug. 2016, pp. 101–106. [Online]. Available: https://ieeexplore.ieee.org/author/37085363693

[31] E. Hernández-Márquez, C. A. Avila-Rea, R. Silva-Ortigoza, J. R. García-Sánchez, M. Antonio-Cruz, H. Taud, and M. Marcelino-Aranda, "Modeling and simulation of a DC motor fed by a full-bridge buck inverter," in *Proc. Int. Conf. Mechatronics, Electron. Automot. Eng. (ICMEAE)*, vol. 21, Nov. 2017, pp. 98–103.

[32] R. C. Dorf and R. H. Bishop, *Modern Control Systems*. London, U.K.: Pearson, 2011.

[33] P. Félix, J. Figueiredo, C. P. Santos, and J. C. Moreno, "Electronic design and validation of powered knee orthosis system embedded with wearable sensors," in *Proc. IEEE Int. Conf. Auto. Robot Syst. Competitions (ICARSC)*, Apr. 2017, pp. 110–115.

[34] N. Merayo, D. Juárez, J. C. Aguado, I. De Miguel, R. J. Durán, P. Fernández, R. M. Lorenzo, and E. J. Abril, "PID controller based on a self-adaptive neural network to ensure QoS bandwidth requirements in passive optical networks," *IEEE/OSA J. Opt. Commun. Netw.*, vol. 9, no. 5, pp. 433–445, May 2017.

[35] T.-Y. Wang and C.-D. Chang, "Hybrid fuzzy PID controller design for a mobile robot," in *Proc. IEEE Int. Conf. Appl. Syst. Invention (ICASI)*, Apr. 2018, pp. 650–653.

[36] W. S. Aboud, S. M. Haris, and Y. Yaacob, "Advances in the control of mechatronic suspension systems," *J. Zhejiang Univ., Sci. C*, vol. 15, no. 10, pp. 848–860, 2014.

[37] A. Vargas-Martínez, L. E. Garza-Castañón, V. Puig, and R. Morales-Menéndez, "Robust MRAC-based fault tolerant control for additive and multiplicative faults in nonlinear systems," *IFAC Proc. Vols.*, vol. 45, no. 20, pp. 540–545, 2012.

[38] A. P. Nair, N. Selvaganesan, and V. R. Lalithambika, "Lyapunov based PD/PID in model reference adaptive control for satellite launch vehicle systems," *Aerosp. Sci. Technol.*, vol. 51, pp. 70–77, Apr. 2016.

[39] P. Jain and M. J. Nigam, "Design of a model reference adaptive controller using modified MIT rule for a second order system," *Adv. Electron. Electr. Eng.*, vol. 3, no. 4, pp. 477–484, 2013.
[40] M. Swathi and P. Ramesh, "Modeling and analysis of model reference adaptive control by using MIT and modified MIT rule for speed control of DC motor," in *Proc. IEEE 7th Int. Adv. Comput. Conf. (IACC)*, Jan. 2017, pp. 482–486.
[41] P. A. Ioannou and J. Sun, *Robust Adaptive Control*. New York, NY, USA: Courier Corporation, 2012.

MOHAMMAD SOLEIMANI AMIRI received the bachelor's degree in mechanical engineering from the Qazvin Islamic Azad University, Iran, in 2011, and the master's degree in mechanical and control system engineering from the Ahrar Institute of Technology and Higher Education, Iran, in 2016. He is currently pursuing the Ph.D. degree in mechanical and control systems engineering with the National University of Malaysia. His research interests include automation, robotics, and control systems.

RIZAUDDIN RAMLI received the bachelor's degree in mechanical engineering from Kyoto University, Japan, in 1997, and the master's degree in mechanical and system engineering and the Ph.D. degree in manufacturing systems from Gifu University, Japan, in 2005 and 2008, respectively. He is currently an Associate Professor with the Department of Mechanical and Materials, Faculty of Engineering and Built Environment, National University of Malaysia. His research interests include Intelligent manufacturing systems, robotics, control, and artificial intelligent.

MOHD FAISAL IBRAHIM received the B.Eng. and M.Eng. degrees in electrical and electronic engineering from Universiti Teknologi Malaysia, in 2002 and 2006, respectively, and the Ph.D. degree from The University of Adelaide, in 2015. He is currently a Senior Lecturer with the Centre for Integrated Systems Engineering and Advanced Technologies (Integra), Universiti Kebangsaan Malaysia (UKM). His research interests are in intelligence systems, evolutionary robotics, and optimization. Since joining UKM, he has been conducting various research works, led a few research grant projects, and has been appointed as an industrial consultant, since 2007.